Journal of Applied Polymer Science

Using Water-Soluble Nickel Acetate as Hole Collection Layer for Stable Polymer Solar Cells

Wenqing Zhang,[1,2] Zhan'ao Tan,[1] Deping Qian,[1] Qi Xu,[1] Liangjie Li,[1] Shusheng Li,[1] Fuzhi Wang,[1] Hua Zheng,[2] Yongfang Li[3]

[1]State Key Laboratory of Alternate Electrical Power System with Renewable Energy Sources, The New and Renewable Energy of Beijing Key Laboratory, North China Electric Power University, Beijing 102206, China
[2]School of Chemical Engineering, Wuhan University of Technology, Wuhan 430070, China
[3]CAS Key Laboratory of Organic Solids, Institute of Chemistry, Chinese Academy of Sciences, Beijing 100190, China
Correspondence to: Z. A. Tan (tanzhanao@ncepu.edu.cn), H. Zheng (zhenghua.whut@126.com), or Y. F. Li (liyf@iccas.ac.cn)

ABSTRACT: We report polymer solar cells (PSCs) based on poly(3-hexylthiophene (P3HT) and [6,6]-phenyl-C_{61}-butyric acid methyl ester (PCBM) using water-soluble nickel acetate ($Ni(CH_3COO)_2$, NiAc) instead of acidic poly(3,4-ethylenedioxythiophene) : poly(styrenesulfonate) (PEDOT : PSS) as hole collection layer (HCL) between the indium tin oxide (ITO) electrode and photoactive layer. The NiAc layer can effectively decrease R_s and increase R_p and shows effective hole collection property. Under the illumination of AM1.5G, 100 mW/cm^2, the short-circuit current density (J_{sc}) of the NiAc based device (ITO/NiAc/P3HT : PCBM/Ca/Al) reach 11.36 mA/cm^2, which is increased by 11% in comparison with that (10.19 mA/cm^2) of PEDOT : PSS based device (ITO/PEDOT : PSS/P3HT : PCBM/Ca/Al). The power conversion efficiency of the NiAc based devices reach 3.76%, which is comparable to that (3.77%) of the device with PEDOT : PSS HCL under the same experimental conditions. Moreover, NiAc based PSCs show superior long-term stability than PEDOT : PSS based PSCs. Our work gives a new option for HCL selection in designing more stable PSCs. © 2012 Wiley Periodicals, Inc. J. Appl. Polym. Sci. 000: 000–000, 2012

KEYWORDS: optical and photovoltaic applications; conducting polymers; films

Received 23 April 2012; accepted 24 June 2012; published online
DOI: 10.1002/app.38251

INTRODUCTION

Polymer solar cells (PSCs), a promising approach to inexpensive solar energy conversion, have drawn great attention in recent years due to the advantages of low cost, light weight, mechanical flexibility, and amenability to manufacture by large-area reel-to-reel coating processes.[1–3] Since the bulk heterojunction (BHJ) concept was reported in 1995,[4,5] great efforts have been made to improve the power conversion efficiency (PCE) of the PSCs using new donor and acceptor photovoltaic materials and new device structures, and recently the PCE has reached 7–8%.[6–10]

In the BHJ-PSC devices, one of the important interfaces is that between the transparent indium tin oxide (ITO) electrode and the photoactive layer, where an interfacial modification layer can both enhance the electric field across the active layer and aid in charge extraction at the contact. Usually, PSC devices use an organic hole collection layer (HCL), poly(3,4-ethylenedioxythiophene) : poly(styrenesulfonate) (PEDOT : PSS), to modulate the interface. The PEDOT : PSS layer serves as a high work-function contact for hole collection. However, the PEDOT : PSS layer is coated from the highly acidic (pH $\sim$ 1) PEDOT : PSS aqueous suspension that corrodes ITO at elevated temperatures and can also diffuse water into active layer, which degrades device performance and causes the problems with respect to morphology uniformity[11–15] and chemical stability.[13–15]

To solve the degradation problem of PEDOT : PSS on ITO, there is an increased interest in developing PSCs with p-type-like metal oxides (such as NiO,[16] MoO_3,[17] V_2O_5,[17] and WO_3[18] with wide band gap, high work function, and good hole conductivity) as the anode modification layer. However, these transition metal oxides are deposited by vacuum based deposition techniques, which is incompatible with solution processing technique in PSCs. Therefore, a solution-processable anode modification layer with low-temperature annealing is in great demand for high-performance PSCs, and the reports about using solution processed transmit metal oxide worked as HCL in PSCs are very limited.[19–23]

In this work, we use water-soluble neutral nickel acetate ($Ni(CH_3COO)_2$, NiAc) instead of the acidic PEDOT : PSS as

HCL between the ITO electrode and poly(3-hexylthiophene : [6,6]-phenyl-C_{61}-butyric acid methyl ester (P3HT : PCBM) photoactive layer. The thermal annealed NiAc layer is highly transparent in the visible range and shows effective hole collection property. Under the illumination of AM1.5G, 100 mW/cm^2, the short-circuit current density (J_{sc}) of the NiAc based device (ITO/NiAc/ P3HT : PCBM/Ca/Al) reach 11.36 mA/cm^2, which is increased by 11% in comparison with that (10.19 mA/cm^2) of PEDOT : PSS based device (ITO/PEDOT : PSS/P3HT : PCBM/Ca/Al). The PCE of the NiAc based device reach 3.76%, which is comparable to that (3.77%) of the device with PEDOT : PSS HCL under the same experimental conditions.

EXPERIMENTAL

Materials

Patterned ITO glass with a sheet resistance of 10 Ω/sq was purchased from China Southern Glass Holding, Co., Ltd. (China). Nickel acetate tetrahydrate ($Ni(CH_3COO)_2{\cdot}4H_2O$, 99.999% purity) was purchased from Alfa Aesar. P3HT (Molecular weight (M_w): 45–60 K via gel permeation chromatography (GPC), Regioregularity: 91–94% via NMR) was purchased from Rieke Metals (USA). $PC_{60}BM$ (99.5% purity) was purchased from Nano-C (USA). PEDOT : PSS (Clevious P VP AI 4083) was purchased from H. C. Stark Company (Germany). All these commercially available materials were used as received without further purification.

Device Fabrication

Device A was fabricated with the structure of glass/ITO/P3HT : PCBM/Ca/Al. Device B was fabricated with the structure of glass/ITO/ PEDOT : PSS/P3HT : PCBM/Ca/Al. Both devices are control devices. Device C was fabricated with the structure of glass/ITO/NiAc/P3HT : PCBM/Ca/Al. The ITO glass was cleaned by sequential ultrasonic treatment in detergent, deionized water, acetone, and isopropanol. The precleaned ITO substrate was treated in an ultraviolet-ozone chamber (Ultraviolet Ozone Cleaner, Jelight Company) for 20 min. PEDOT : PSS aqueous solution was filtered through a 0.45-μm filter and spin coated at 2000 rpm for 60 s on the ITO electrode. Subsequently, the PEDOT : PSS film was baked at 150°C for 10 min in air. The thickness of PEDOT : PSS was around 30 nm. NiAc buffer layer was prepared by spin coating (1000–4000 rpm) a 1.5 mg/mL nickel acetate tetrahydrate aqueous solution on the precleaned ITO substrate and then baked at 150°C for 10 min to remove water of hydration in air. Subsequently, the substrate was transferred to a nitrogen-filled glove-box, and the photosensitive blend layer was prepared by spin coating (600–1000 rpm) the 1,2-dichlorobenzene solution of P3HT and PCBM (1 : 1 w/w, polymer concentration of 20 mg/mL) on the modified ITO electrode for 30 s, and then dried in covered glass Petri dishes for slow growth the active layer. Finally, the substrate was transferred to a vacuum chamber and a 10 nm of Ca and 100 nm of Al was thermally deposited on the photoactive layer under a base pressure of 5×10^{-5} Pa. The active area of the device is about 4 mm^2.

Device Characterization

The current density–voltage (J–V) measurement of the devices was conducted on a computer-controlled Keithley 236 Source Measure Unit (SMU). Device characterization was done in a glove-box under simulated AM1.5G irradiation (100 mW/cm^2) using a xenon-lamp-based solar simulator (from Newport). The incident photon to converted current efficiency (IPCE) was measured using a Stanford Research Systems model SR830 digital signal processing (DSP) lock-in amplifier coupled with a WDG3 monochromator and 500 W xenon lamp. The light intensity at each wavelength was calibrated with a standard single-crystal Si photovoltaic cell. All the measurements were performed under ambient atmosphere at room temperature.

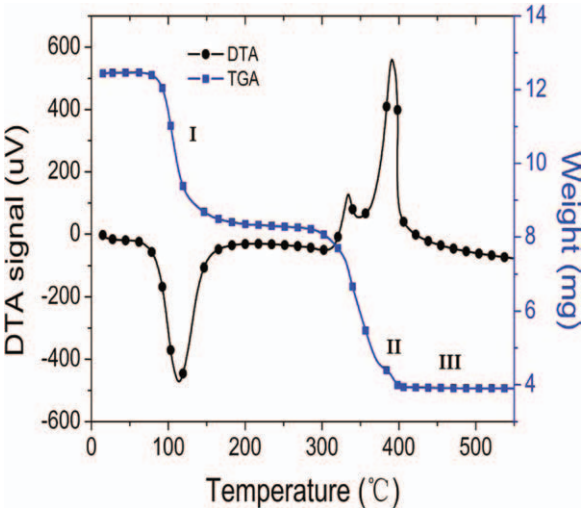

Figure 1. Thermogravimetric and DTA of nickel acetate tetrahydrate. [Color figure can be viewed in the online issue, which is available at wileyonlinelibrary.com.]

Instrumentation

Thermogravimetric analysis (TGA) and differential thermal analysis (DTA) was conducted on a Perkin-Elmer 7 thermogravimetric analyzer with a heating rate of 20°C/min under ambient atmosphere. The transmittance spectra were recorded using an HP8453 UV–vis spectrometer. The surface morphologies and phase changes of the modification layer on ITO and the active layers were analyzed using a VEECO DICP-II atomic force microscope operated in the tapping mode. The thickness of the film involved in the device was measured by Ambios Technology XP-2 surface profilometer. Cyclic voltammogram curves were recorded on a Zahner IM6e electrochemical workstation with a scan speed of 100 mV/s, using glassy carbon disks as the working electrode (area ca. 0.25 cm^2), a Pt wire as the counter electrode, and a Ag/Ag^+ as reference electrode in 0.1M tetrabutylammonium hexafluorophosphate (Bu_4NPF_6) acetonitrile solution. A 1.5 mg/mL nickel acetate tetrahydrate aqueous solution was dropped on the working electrode and then baked at 150°C for 10 min in air.

RESULTS AND DISCUSSION

TGA of NiAc Precursor

The decomposition behavior of the precursor nickel acetate tetrahydrate ($Ni(CH_3COO)_2{\cdot}4H_2O$) was studied by TGA and DTA at a scan rate of 20°C/min, in the temperature range 20–550°C. Figure 1 shows the TGA and DTA analysis of $Ni(CH_3COO)_2{\cdot}4H_2O$ in air atmosphere. The TGA curve displays three weight loss steps that are labeled as steps I–III. The first step (I) at 87–160°C is accompanied by a weight loss of 30%. This step

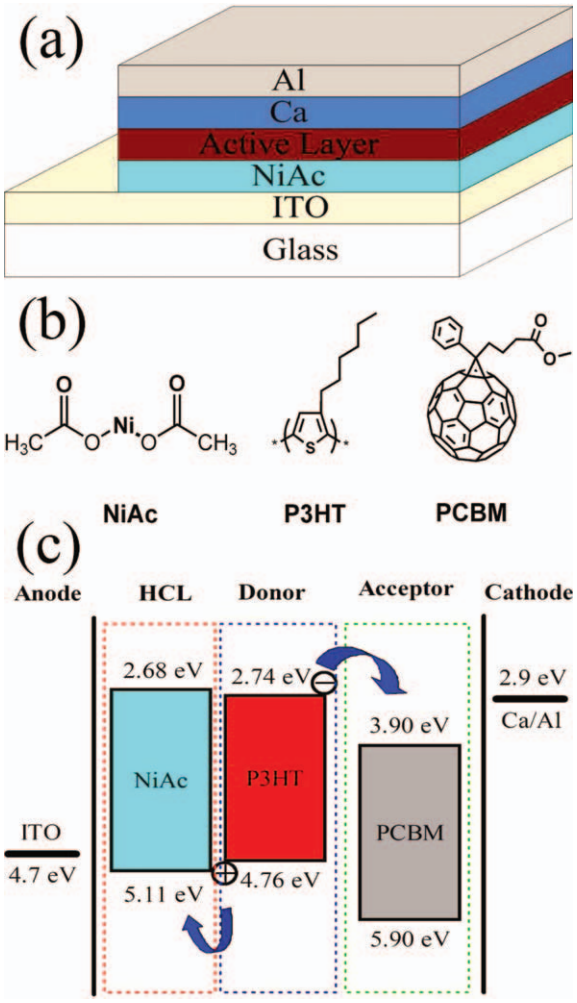

Figure 2. (a) Device structure of the PSCs. (b) Molecular structures of P3HT, PCBM, and NiAc. (c) The HOMO and LUMO energy levels of the materials involved in the PSCs. [Color figure can be viewed in the online issue, which is available at wileyonlinelibrary.com.]

represents the dehydration process of the salt tetrahydrate (where $4H_2O$ = 29% of the molecular weight of [$Ni(CH_3COO)_2{\cdot}4H_2O$]). A second weight loss step of about 33% appeared at 280–380°C. The third, and last, step (III) takes place in the temperature range 380–440°C and is accompanied by a loss in weight of about 6%. The DTA curve shows three peaks. The first peak is located at 114°C and is attributed to the dehydration of the tetrahydrate salt. The second peak is located at 334°C, which indicates that the decomposition of anhydrous nickel acetate. The third peak located at 391°C corresponds to step (III) in the TGA curve, which could be attributed to the decomposition of some NiO to Ni metal. Our observations from TGA and DTA are in good agreement with previous studies reported in literatures.[24,25] So in our case (annealing at 150°C for 10 min in air), the precursor should only release the lattice water and could not transit to nickel oxide.

Structure Design of the PSCs

The sandwiched structure of glass/ITO/NiAc/P3HT : PCBM/Ca/Al is used in fabrication of the PSCs, with ITO as positive electrode, NiAc as hole collection interface layer, P3HT : PCBM as photoactive layer, and Ca/Al as negative electrode. The device structure of PSC is given in Figure 2(a) and the molecular structures of P3HT, PCBM, and NiAc are shown in Figure 2(b).

Figure 2(c) shows the energy levels of the materials involved in the PSCs. The energy level of NiAc was determined by electrochemical cyclic voltammetry. The electronic energy levels of P3HT[26] and PCBM[27] were taken from literatures. When light irradiates on the photoactive layer through ITO electrode, the active layer will absorb photons to produce excitons, and the excitons will diffuse toward and dissociate at the P3HT/PCBM interface into electrons in the lowest unoccupied molecular orbital (LUMO) of the acceptor PCBM and holes in the highest occupied molecular orbital (HOMO) of the donor P3HT. As the HOMO level (–5.11 eV) of NiAc is 0.35 eV lower than that of P3HT, holes can transport to ITO electrode through NiAc. But the LUMO level (–2.68 eV) of NiAc is much higher than that (–3.90 eV) of PCBM, so that it blocks the electron transport from PCBM to the ITO electrode. Thus, from the viewpoint of energy levels, the device could show high charge collection efficiencies on both electrodes.[28]

The Transmittance of the Buffer Layer

The transmittance of the buffer layer on the ITO electrode is an important parameter to affect the incident light from ITO side. Figure 3 shows the optical transmittance spectra of NiAc and its counterpart PEDOT : PSS on ITO coated glass. The integral of transmittance from 300 to 900 nm for ITO/NiAc is 98.2% of that for bare ITO, and 98.4% of that for ITO/PEDOT : PSS, showing highly transparent. Moreover, the transmittance of ITO/NiAc at the wavelength between 500 and 900 nm is a little higher than that of ITO/PEDOT : PSS, which will benefit increasing the photocurrent of device in the longer wavelength range.

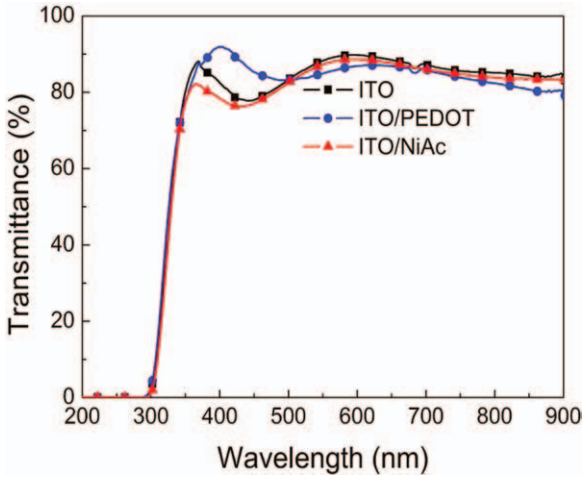

Figure 3. Optical transmittance spectra of PEDOT : PSS and NiAc modification layer after 150°C annealing for 10 min on ITO coated glass. [Color figure can be viewed in the online issue, which is available at wileyonlinelibrary.com.]

Applied Polymer SCIENCE

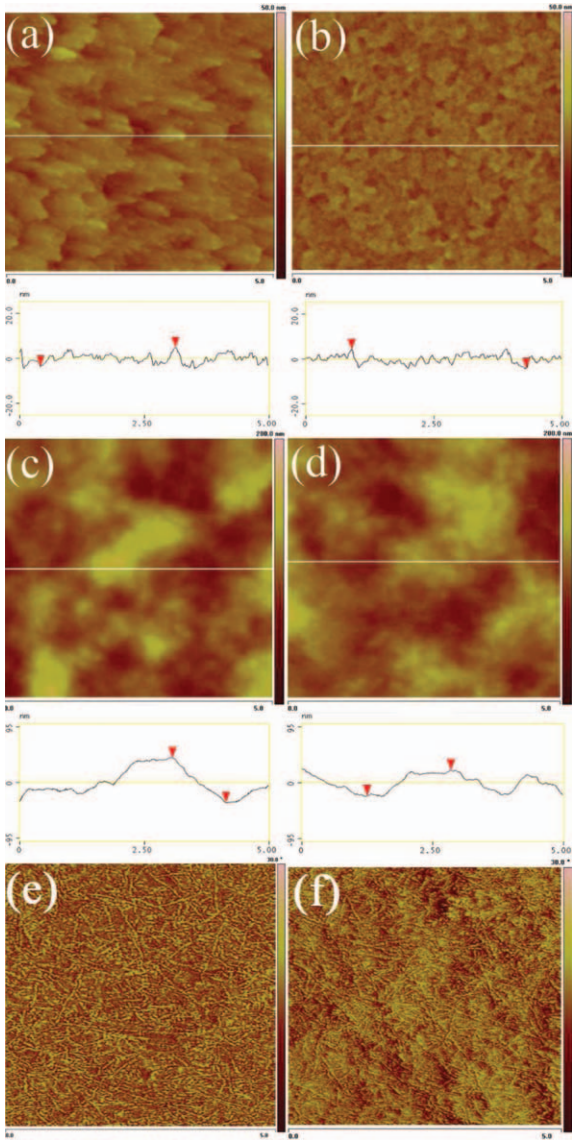

Figure 4. AFM height images of (a) NiAc on ITO after 150°C annealing for 10 min, (b) PEDOT : PSS on ITO after 150°C annealing for 10 min, (c) P3HT : PCBM (1 : 1 wt %) on ITO/NiAc substrate, and (d) P3HT : PCBM (1 : 1 wt %) on ITO/PEDOT : PSS substrate. AFM phase images of (e) P3HT : PCBM (1 : 1 wt %) on ITO/NiAc substrate and (f) P3HT : PCBM (1 : 1 wt %) on ITO/PEDOT : PSS substrate. The scan size is 5 × 5 μm^2. [Color figure can be viewed in the online issue, which is available at wileyonlinelibrary.com.]

The Morphology of the Thin Films

The tapping mode atomic force microscopy (AFM) image at the 5 × 5 μm^2 scan size of NiAc interface layer on ITO after 150° annealing for 10 min was illustrated in Figure 4(a). The root mean square (rms) roughness of the NiAc layer was 2.1 nm, which is comparable with that (1.8 nm) of PEDOT : PSS on ITO substrate as shown in Figure 4(b). Figure 4(c) shows the AFM image of the surface of the P3HT : PCBM (1 : 1 w/w) active layer on ITO/NiAc substrate with a rms roughness of 13.1 nm, which is a little higher than that (10.9 nm) of P3HT : PCBM on ITO/PEDOT : PSS substrate as shown in Figure 4(d). This might be ascribed to the higher surface energy of NiAc layer than that of PEDOT : PSS layer.[9] On both NiAc and PEDOT : PSS substrates, the P3HT : PCBM layer has much larger roughness than that of the substrate. The increase in

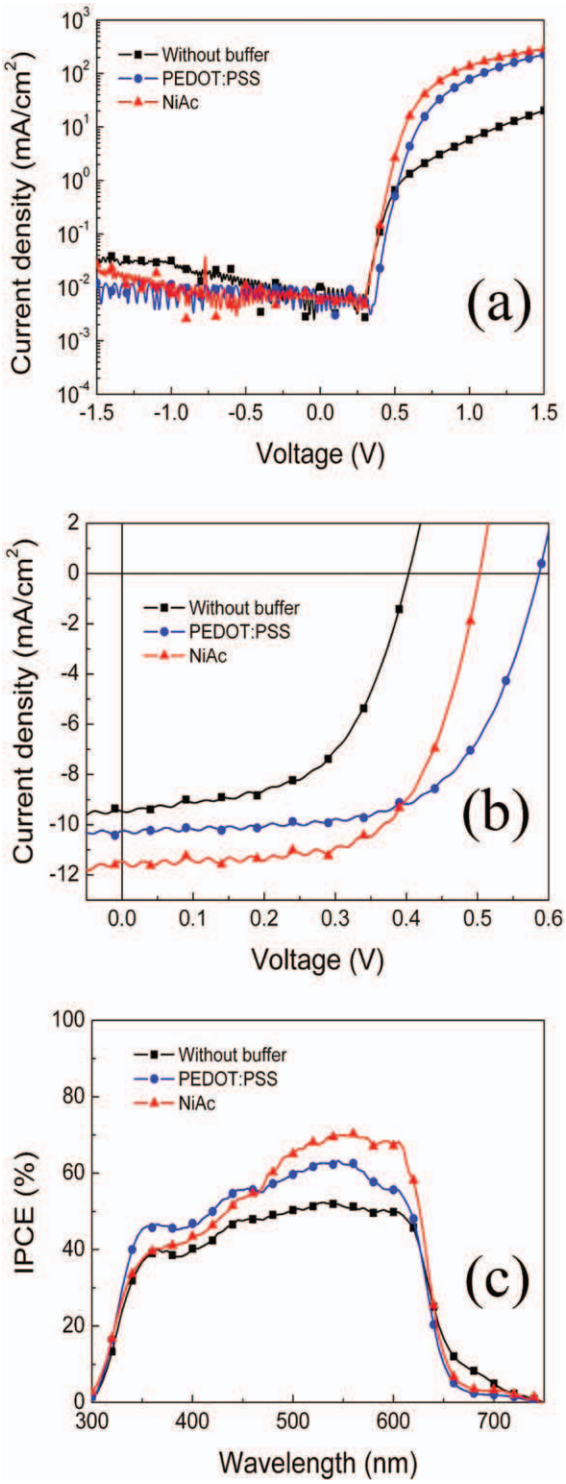

Figure 5. (a) Semilogarithmic *J–V* curves of the PSCs in the dark. (b) *J–V* curves of the PSCs under the illumination of AM1.5G, 100 mW/cm^2. (c) IPCE spectra of the PSCs. [Color figure can be viewed in the online issue, which is available at wileyonlinelibrary.com.]

Table I. Device Parameters of the PSCs with Different HCL in the Dark and under 100 mW/cm^2 Illumination

Devices	V_{oc} (V)	J_{sc} (mA/cm^2)	FF (%)	PCE (%)	R_p[a] (kΩ cm^2)	R_s[a] (Ω cm^2)
No buffer (A)	0.40	9.48	56.9	2.16	42.3	65.7
PEDOT : PSS (B)	0.59	10.19	62.7	3.77	93.6	4.2
NiAc (C)	0.50	11.36	66.2	3.76	177.8	3.1

[a]Parallel resistance (R_p) and series resistance (R_s) for PSCs in the dark are obtained at around 0 and 1 V, respectively.

roughness is attributed to P3HT self-organization and phase separation of the blend as shown in Figure 4(e) and (f).[29] P3HT chains self-organizing into ordered structure can significantly enhance the hole mobility, and the aggregation of PCBM molecules can form separate paths for electron transport.[29]

Comparative Studies of the PSCs with Different HCL

To investigate the NiAc HCL effect on the photovoltaic performance of PSCs, we design three kinds of devices structures: (A) ITO/P3HT : PCBM (240 nm)/Ca (10 nm)/Al (100 nm), (B) ITO/PEDOT : PSS (30 nm)/ P3HT : PCBM (240 nm)/Ca (10 nm)/Al (100 nm), and (C) ITO/NiAc (12 nm)/ P3HT : PCBM (240 nm)/Ca (10 nm)/Al (100 nm). For the current density–voltage (J–V) curves measured with a computer-controlled Keithley 236 SMU in the dark [Figure 5(a)], the rectification ratio at ±1.0 V of Device A and B is 2.2 × 10^2 and 6.9 × 10^3, respectively. Whereas that of NiAc based Device C reach 1.5 × 10^4, two order higher than that of Device A without HCL, and it is two times of that of Device B with PEDOT : PSS HCL. The higher rectification ratio of the NiAc based Device C results from the higher injection current at the positive voltage and lower leakage current at the negative voltage.

J–V curves of Devices A–C under the illumination of AM 1.5 G, 100 mW/cm^2 are shown in Figure 5(b), and the device performance parameters (average of 12 devices) are summarized in Table I. For Device A without HCL, it shows a PCE of 2.16%, a short-circuit current density (J_{sc}) of 9.48 mA/cm^2, an open-circuit voltage (V_{oc}) of 0.40 V, and a fill factor (FF) of 56.9%. In contrast, the four parameters, V_{oc}, J_{sc}, FF, and PCE, for Device C with NiAc HCL are all enhanced to 0.50 V, 11.36 mA/cm^2, 66.2%, and 3.76%, respectively. In comparison with Device B with PEDOT : PSS HCL, both J_{sc} and FF are increased, whereas the V_{oc} is slightly decreased, and the overall PCE is almost the same. The increased J_{sc} of Device C could be ascribed to enhanced conductivity and the spatially redistributing of the light intensity inside the device caused by NiAc modification layer in the device.[30,31] The slightly increased FF of Device C could result from the decrease in series resistance (R_s) from 4.2 to 3.1 Ω cm^2 and greatly increase in parallel resistance (R_p) from 93.6 to 177.8 kΩ cm^2 for PEDOT : PSS and NiAc modified device, respectively.[32] The slightly decreased V_{oc} of Device C could result from the higher HOMO level (−5.11 eV) of NiAc than that (−5.30 eV) of PEDOT : PSS as shown in Figure 2(c).[33] Another possibility for lower V_{oc} of NiAc based device should attribute to the surface energy difference between the NiAc layer and the PEDOT : PSS layer as shown in Figure 4, which can affect the wettability of the photoactive layer with the contact buffer layer.[9]

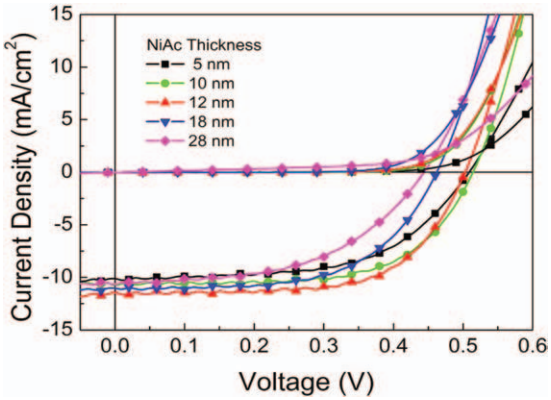

Figure 6. J–V curves of the PSCs with different NiAc thicknesses in the dark and under the illumination of AM1.5G, 100 mW/cm^2. [Color figure can be viewed in the online issue, which is available at wileyonlinelibrary.com.]

We compared the IPCE spectra of Devices A–C, as shown in Figure 5(c). The IPCE results agree with the J_{sc} of the PSCs mentioned earlier. The higher IPCE of Device C could also be ascribed to enhanced transmittance of ITO/NiAc at the wavelength over 500 nm (as shown in Figure 3) and the good crystallized morphology of blend film as shown in Figure 4.

Effect of NiAc Layer Thickness on the Performance of the PSCs

The current–voltage (J–V) characteristics for the PSCs with different NiAc thicknesses in the dark and under the illumination of AM1.5G, 100 mW/cm^2, are shown in Figure 6. Their photovoltaic properties are summarized in Table II (average of 12 devices). It can be seen, there is a trade off between the parallel resistance (R_p) and series resistance (R_s). Thicker NiAc layer can block more leakage-current caused by pinhole or other defects,[34] causing R_p (from 45.3 to 177.8 kΩ cm^2) and FF enhancement. However, thicker NiAc will increase R_s (from 3.1 to 15.7 Ω cm^2), because the conductivity of NiAc is limited, and this will decrease J_{sc}.[35,36] The optimal thickness of NiAc layer is about 10–15 nm. The V_{oc}, J_{sc}, FF, and PCE for the best device with 12-nm NiAc layer is 0.50 V, 11.36 mA/cm^2, 66.2%, and 3.76%, respectively.

Table II. Device Parameters of PSCs with Different NiAc Thickness in the Dark and under the 100 mW/cm^2 Illumination

NiAc (nm)	V_{oc} (V)	J_{sc} (mA/cm^2)	FF (%)	PCE (%)	R_p[a] (kΩ cm^2)	R_s[a] (Ω cm^2)
5	0.51	10.06	57.9	2.97	45.3	11.2
10	0.51	10.80	62.6	3.45	113.4	4.5
12	0.50	11.36	66.2	3.76	177.8	3.1
18	0.46	11.01	60.0	3.04	108.5	4.6
28	0.44	10.71	51.2	2.41	1.2	15.7

[a]Parallel resistance (R_p) and series resistance (R_s) for PSCs in the dark are obtained at around 0 and 1 V, respectively.

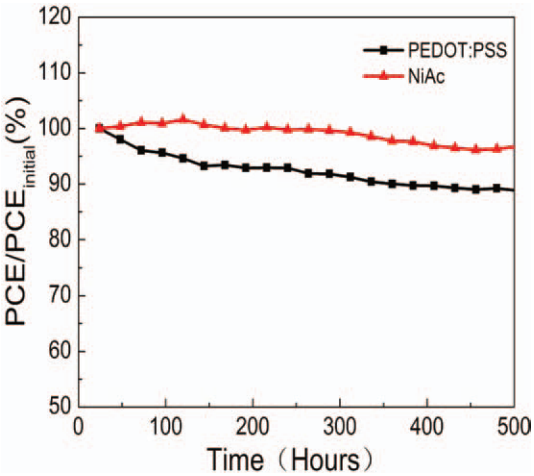

Figure 7. Long-term stability of the PCE of PSCs based on either PEDOT : PSS or NiAc HCLs. The devices have been stored in N_2 filled glove-box. [Color figure can be viewed in the online issue, which is available at wileyonlinelibrary.com.]

To investigate the effect of HCL on the long-term stability of PSCs, we tested the PCE degradation of nonencapsulated devices based on PEDOT : PSS and NiAc over time in a nitrogen filled glove-box. As shown in Figure 7, PCE of the PEDOT : PSS modified cells decay ~12% of the original value after storage in nitrogen for 500 h, whereas that of NiAc modified cells only decay ~4% of the original value after storage in nitrogen for the same time. These results indicate nonacidic NiAc HCL can effectively improve the long-term stability of the PSCs.

CONCLUSIONS

In conclusion, we demonstrate stable PSCs based on P3HT : PCBM using water-soluble neutral NiAc instead of acidic PEDOT : PSS as HCL. The NiAc layer can effectively decrease R_s and increase R_p, and shows effective hole collection property. Under the illumination of AM1.5G, 100 mW/cm^2, the NiAc based device shows a PCE of 3.76%, which is comparable to that (3.77%) of the device with PEDOT : PSS HCL under the same experimental conditions. This work gives a new option for HCL selection in designing more stable PSCs.

ACKNOWLEDGMENTS

The work was supported by the NSFC (Nos. 21004019, 51173040, 91023039, and 21021091), the Ministry of Science and Technology of China (863 project, No. 2011AA050523), and the Chinese Academy of Sciences. Z. Tan thanks the financial support from the Beijing NOVA Program (No. 2010B038), SRFDP (No. 20100036120007), and Fundamental Research Funds for the Central Universities, China (10MG32).

REFERENCES

1. Gunes, S.; Neugebauer, H.; Sariciftci, N. S. *Chem. Rev.* **2007,** *107*, 1324.
2. Chen, J.; Cao, Y. *Acc. Chem. Res.* **2009,** *42*, 1709.
3. Li, Y. F. *Acc. Chem. Res.*, **2012**, *45*, 723.
4. Yu, G.; Hummelen, J.; Wudl, F.; Heeger, A. J. *Science* **1995,** *270*, 1789.
5. Halls, J. J. M.; Walsh, C. A.; Greenham, N. C.; Marseglia, E. A.; Friend, R. H.; Moratti, S. C.; Holmes, A. B. *Nature* **1995,** *376*, 498.
6. Chen, H. Y.; Hou. J. H.; Zhang, S. Q.; Liang, Y. Y.; Yang, G. W.; Yang, Y.; Yu, L. P.; Wu, Y.; Li, G. *Nat. Photonics* **2009,** *3*, 649.
7. Liang, Y.; Xu, Z.; Xia, J.; Tsai, S. T.; Wu, Y.; Li, G.; Ray, C.; Yu, L. *Adv. Mater.* **2010,** *22*, E135.
8. Huo, L. J.; Zhang, S. Q.; Guo, X.; Xu, F.; Li, Y. F.; Hou, J. H. *Angew. Chem. Int. Ed. Engl.* **2011,** *50*, 9697.
9. Tan, Z.; Zhang, W.; Zhang, Z.; Qian, D.; Huang, Y.; Hou, J.; Li, Y. *Adv. Mater.* **2012,** *24*, 1476.
10. He, Z.; Zhong, C.; Huang, X.; Wong, W. Y.; Wu, H.; Chen, L.; Su, S.; Cao, Y. *Adv. Mater.* **2011,** *23*, 4636.
11. Jong, M. P.; IJzendoorn, L. J.; Voigt, M. J. A. *Appl. Phys. Lett.* **2000,** *77*, 2255.
12. Dang, X. D.; Dante, M.; Nguyen, T. Q. *Appl. Phys. Lett.* **2008,** *93*, 241911.
13. Nardes, A. M.; Kemerink, M.; Kok, M. M.; Vinken, E.; Maturova, K.; Janssen, R. A. *J. Org. Electron.* **2008,** *9*, 727.
14. Norrman, K.; Madsen, M. V.; Gevorgyan, S. A.; Krebs, F. C. *J. Am. Chem. Soc.* **2010,** *132*, 16883.
15. Norrman, K.; Gevorgyan, S. A.; Krebs, F. C. *ACS Appl. Mater. Interfaces* **2009,** *1*, 102.
16. Irwin, M. D.; Buchholz, B.; Hains, A. W.; Chang, R. P. H.; Marks, T. *J. Proc. Natl. Acad. Sci. U. S. A.* **2008,** *105*, 2783.
17. Shrotriya, V.; Li, G.; Yao, Y.; Chu, C.; Yang, Y. *Appl. Phys. Lett.* **2006,** *88*, 073508.
18. Han, S.; Shin, W. S.; Seo, M.; Gupta, D.; Moon, S. J.; Yoo, S. *Org. Electron.* **2009,** *10*, 791.
19. Hammond, S. R.; Meyer, J.; Widjonarko, N. E.; Ndione, P. F.; Sigdel, A. K.; Garcia, A.; Miedaner, A.; Lloyd, M. T.; Kahn, A.; Ginley, D. S.; Berrya, J. J.; Olsona, D. C. *J. Mater. Chem.* **2012,** *22*, 3249.
20. Steirer, K. X.; Ndione, P. F.; Widjonarko, N. E.; Lloyd, M. T.; Meyer, J.; Ratcliff, E. L.; Kahn, A.; Armstrong, N. R.; Curtis, C. J.; Ginley, D. S.; Berry, J. J.; Olson, D. C. *Adv. Energy Mater.* **2011,** *1*, 813.
21. Chen, C.; Chen, Y.; Chuang, S.; Adv. *Mater.* **2011,** *23*, 3859.
22. Girotto, C.; Voroshazi, E.; Cheyns, D.; Heremans, P.; Rand, B. P. *ACS Appl. Mater. Interfaces* **2011,** *3*, 3244.
23. Sun, Y.; Takacs, C. J.; Cowan, S. R.; Seo, J.; Gong, X.; Roy, A.; Heeger, A. J. *Adv. Mater.* **2011,** *23*, 2226.
24. Lee, Y. S.; Sun, Y. K.; Nahm, K. S. *Solid State Ionics* **1999,** *118*, 159.
25. Jesus, J. C.; Gonzalez, I.; Quevedo, A.; Puerta, T. *J. Mol. Catal. A: Chem* **2005,** *228*, 283.
26. Hou, J. H.; Tan, Z. A.; Yan, Y.; He, Y. J.; Yang, C. H.; Li, Y. F. *J. Am. Chem. Soc.* **2006,** *128*, 4911.

27. He, Y. J.; Zhao, G. J.; Peng, B.; Li, Y. F. *Adv. Funct. Mater.* **2010,** *20*, 3383.

28. Hoppe, H.; Niggemann, M.; Winder, C.; Kraut, J.; Hiesgen, R.; Hinsch, A.; Meissner, D.; Sariciftci, N. S. *Adv. Funct. Mater.* **2004,** *14*, 1005.

29. Li, G.; Shrotriya, V.; Huang, J.; Yao, Y.; Moriarty, T.; Emery, K.; Yang, Y. *Nat. Mater.* **2005,** *4*, 864.

30. Kim, J. Y.; Kim, S. H.; Lee, H. H.; Lee, K.; Ma, W. L.; Gong, X.; Heeger, A. J. *Adv. Mater.* **2006,** *18*, 572.

31. Hänsel, H.; Zettl, H.; Krausch, G.; Kisselev, R.; Thelakkat, M.; Schmidt, H. W. *Adv. Mater.* **2003,** *15*, 2056.

32. Tan, Z.; Yang, C.; Zhou, E.; Wang, X.; Li, Y. *Appl. Phys. Lett.* **2007,** *91*, 023509.

33. Vandewal, K.; Tvingstedt, K.; Gadisa, A.; Inganäs, O.; Manca, J. V. *Nat. Mater.* **2009,** *8*, 904.

34. Dongaonkar, S.; Servaites, J. D.; Ford, G. M.; Loser, S.; Moore, J.; Gelfand, R. M.; Mohseni, H.; Hillhouse, H. W.; Agrawal, R.; Ratner, M. A.; Marks, T. J.; Lundstrom, M. S.; Alam, M. A. J. *Appl. Phys.* **2010,** *108*, 124509.

35. Steim, R.; Choulis, S. A.; Schilinsky, P.; Brabec, C. J. *Appl. Phys. Lett.* **2008,** *92*, 093303.

36. Waldauf, C.; Morana, M.; Denk, P.; Schilinsky, P.; Coakley, K.; Choulis, S. A.; Brabec, C. J. *Appl. Phys. Lett.* **2006,** *89*, 233517.